Oligocene to present shallow subduction beneath the southern Puna plateau

Guido M. Gianni[1], Héctor P. A. García[2], Agustina Pesce[2], Marianela Lupari[2], Marcelo González[2], Laura Giambiagi[3].

[1] Instituto de Estudios Andinos Don Pablo Groeber, UBA-CONICET, Departamento de Ciencias Geológicas, FCEN, Laboratorio de Geodinámica. Universidad de Buenos Aires, Argentina. Email: guidogianni22@gmail.com

[2] IGSV. Instituto Geofísico Sismológico Ing. Volponi. Universidad Nacional de San Juan. CONICET. guidogianni22@gmail.com

[3] IANIGLA, CCT Mendoza, CONICET, Mendoza, Argentina

ABSTRACT

The southern Puna plateau is a conspicuous example of a high-elevation orogenic plateau in a non-collisional setting. This orogenic sector is currently located above an anomalously shallow subduction segment, in which timing and relation to upper-plate tectonics have been widely overlooked. This subduction segment, here referred to as the southern Puna shallow subduction (SPSS), is characterized by a ~200 km wide shallow area located at ~300 km from the trench at a depth of ~100-120 km and dipping 10-12° to the east. To determine the onset of the SPSS and its link to the tectonic and magmatic activity in this region, we analyzed the tectonomagmatic record of the southern Puna plateau from preexisting datasets. Also, we present a new approach based on global subduction data that provides a straightforward methodology to extract potential paleo-slab angles from the bedrock arc record. This analysis reveals that a pronounced eastward arc-front migration and magmatic broadening took place at ~26 Ma and was preceded by ~ 4 Ma of reduced magmatic activity, which we link to the inception of the SPSS. As expected in shallow subduction settings, a change to basement-cored distributed deformation south of 25°S in the southern Puna plateau coincides with the beginning of shallow subduction. Also, the SPSS is coincident with the enigmatic post-Eocene intraplate deformation of the Otumpa Hills located at ~950 km from the trench. We suggest that this succession of events is not fortuitous and that the development of the SPSS impacted directly the overriding plate since the Oligocene contributing to the building of one of the largest topographies (>3 km) and thickest orogenic crusts (~70-60 km) on Earth. The shallow subduction would have acted jointly with Cenozoic changes in plate kinematics and climate enhancing Andean orogenesis at studied latitudes.

Keywords: Central Andes, Puna plateau, shallow subduction, broken foreland.

1. INTRODUCTION

Flat-slab subduction is characterized by 5° dipping to horizontal angles beyond the seismogenic zone at a depth of ~100 km (Barazangi and Isacks, 1976). During slab flattening, the volcanic front migrates and the bulk arc broadens towards the continental interior and then shuts-off (Dickinson and Snyder, 1978; Coney and Reynolds, 1979) (Fig. 1). Extinction of arc magmatism is attributed to the suppression of the mantle wedge due to slab flattening (Barazangi and Isacks, 1976). However; there are exceptions, known from current settings (e.g. SW Japan, Gutscher and Peacok, 2003) and the geologic record (e.g. Late Cretaceous shallow subduction in the Southern Central Andes, Ramos and Folguera, 2005; Neogene Payenia shallow subduction in the Southern Central Andes, Kay and

Copeland, 2006; Ecuador Neogene shallow subduction, Schüte et al., 2010; Neogene shallow subduction in the Northern Patagonian Andes, Orts et al., 2012; among others), in which arc broadening does not evolve into a magmatic lull. The latter case has been interpreted, when other factors discarded (e.g., arc migration due to subduction erosion), as shallow subduction with intermediate angles between normal (~30°) and flat, usually between 20° and 10°. Parametric studies based on the analysis of subduction zones around the globe have recognized a link between slab dip angle and upper-plate deformation, with lower angles correlating with backarc shortening (Jarrard, 1986; Lallemand et al., 2005; Schellart et al., 2008) (Fig. 1). In the case of very low slab angles, as those associated with flat and shallow subduction, an even greater coupling between the upper and subducting plates is expected (Martinod et al., 2010) often leading to basement-cored distributed deformation or broken foreland/Laramide-style of deformation as commonly referred in these settings (e.g. Jordan and Allmendinguer, 1986; Gutsher et al., 2000; Gianni et al., 2018a,b) (Fig. 1). Stress transmission and interplate basal shear in low angle subduction settings is able to produce intraplate deformation leading to basement-involved tectonic and kilometric-scale block uplift between 600 and 1500 km from the trench (e.g. Snyder and Dickinson, 1978; Ramos et al., 2002). The only known exception to this is the Mexican flat-slab. The latter is not associated with significant upper plate contraction and has been explained by a low interplate coupling caused by highly hydrated rocks at the plates contact (e.g. Manea et al., 2017). Flat subduction also affects the thermal state of the upper-plate as revealed by medium to low heat-flow values (e.g. Sánchez et al., 2018). The latter is thought to favor distal stress transmission and deformation in these settings (Gutcher et al. 2000).

Two of the best-known cases of active flat subduction were found in the late seventies in the western margin of South America. These are the Peruvian (5°-14°S) and the Chilean flat-slabs (27°30º-33°30'S) (see Ramos and Folguera, 2009 for a review) (Fig. 2A). Andean flat-slab segments are bounded by three active magmatic arc regions known as the Northern, Central and Southern volcanic zones in sectors of normal angle subduction, dipping on average 30°E (Barazangi and Isacks, 1976). The Central volcanic zone (CVZ), between the Peruvian and Chilean flat-slabs, is placed on the Altiplano-Puna plateau, the largest non-collisional orogen on Earth (Oncken et al., 2006) (Fig. 2A). The CVZ is characterized by a southern region in the Puna plateau overlying a shallower slab angle between 24°S to 27°30'S, first noticed by Cahill and Isacks (1992) and further documented in more recent works (e.g. Bianchi et al., 2013; Mulcahy et al, 2014; Álvarez et al., 2015) (Figs. 2B,C). This zone contrasts with the abrupt flat to normal subduction transitions usually described in the Nazca plate (Cahill and Isacks, 1992; Scire et al., 2014, 2015). Although observed in previous studies, the occurrence of this low angle subduction segment in the CVZ and its potential relation to upper-plate deformation in the Puna plateau have been largely overlooked. The development of this slab geometry could have had a significant impact on the tectonic and topographic evolution of the southern Puna plateau associated with one of the thickest crusts on Earth. For instance, a similar slab angle inferred through magmatic proxies for the ancient Payenia shallow subduction zone (18-5 Ma) has been linked to cordilleran uplift and intraplate contraction in the Southern Central Andes between 35°S and 38°S (Kay and Copeland, 2006; Ramos et al., 2014).

With a plethora of new geological information published in the last decade it is timely to reexamine the question of shallow subduction beneath the southern Puna. Hence, we review and analyze preexisting geological data and integrate it into a new geodynamic model linking the southern Puna shallow subduction and the tectonic evolution of the Andes in the southern Puna plateau. For this, we first compare this anomalously shallow segment with the Nazca plate geometry beneath the northern CVZ. Then, we analyze the Cenozoic tectonomagmatic record as a proxy of geodynamic changes in the active margin (Coney and Reynolds, 1977) to unravel the beginning of shallow subduction and its potential influence on mountain-building. To track the evolution of slab angles though the Cenozoic, we used a new approach based on the application of empirical relations between arc-trench distance and slab angles from current global subduction zones. We demonstrate that this shallow subduction segment constitutes an ancient configuration that coexisted with major deformation and crustal thickening and explains several key features in the evolution of the southern Puna plateau.

2. METHODOLOGY

To compare the subduction segment below the southern Puna plateau with the rest of the Andean subduction zone beneath the CVZ we extract profiles (P1 to 13) from the recent Slab2 global subduction zone model (Hayes et al., 2018) (Fig. 3A). The Slab2 is a new model that describes the 3D geometries of all seismically active subduction zones worldwide from the near-surface (oceanic trenches for most slabs) to the upper mantle and hence, constitutes a suitable tool to analyze in detail the subduction zone below the CVZ.

To understand the potential relation between the tectonic evolution of the southern Puna and the development of the SPSS, we carry out a synthesis of the Andean deformation and the related sedimentary basin evolution between 24’30° to 27°30’S. Additionally, we studied the spatiotemporal magmatic arc behavior as a proxy of dynamic changes in the Andean subduction during the Paleogene to present stages of Andean orogenesis. The spatiotemporal magmatic evolution is usually considered an indirect indicator of subduction processes such as increase/decrease in plate coupling manifested on subduction erosion/accretion (von Huene & Scholl, 1991) and variations in slab dip (Coney & Reynolds, 1977).

To unravel potential paleo-slab angles throughout the subduction history of the study area, we used a new method based on the application of an arc-trench distance vs. slab angle diagram including a current global subduction dataset (Perrin et al., 2018). By means of this diagram, we compare paleo-arc-trench distances at different times to obtain potential paleo-slab angles below the arc region.

3. THE SOUTHERN PUNA SHALLOW SUBDUCTION

Sections in fig. 3B show that profiles P10 to P13 describe a slab shallowing that begins at about ~300 km from the trench that is characterized by a ~200 km wide shallow portion at ~100-120 km that dips between 10 to 12° to the east (Fig. 3B). A comparison between profiles P10 to P13 with the first profile describing a normal angle (i.e. P8) in the northern CVZ, shows that the overall slab located over the southern Puna plateau is ~30 to ~90 km shallower than the slab in those areas to the north (Fig. 3B).

This geometrical signature and the existence of an active arc zone allow to classify this segment as a shallow subduction configuration similar to those suggested in current settings (e.g. Cascadia and Shikoku subduction zones, Gutscher et al., 2000) and inferred in the past from spatio-temporal analysis of arc magmatism (e.g. Kay and Copeland, 2006; Folguera and Ramos, 2011). In this study, we refer to this subduction segment as the southern Puna shallow subduction (SPSS).

4. DEFORMATION AND MAGMATISM IN THE SOUTHERN PUNA PLATEAU

4.1. Deformational history of the southern Puna plateau

The Central Andean plateau is characterized by a high elevation (>3 km), high upper plate shortening (up to 270 km), significant crustal thickening (70-60 km) and active magmatism, and is delimited to the north and south by arc-gaps linked to the Peruvian and Chilean flat-slab segments (e.g. Oncken et al., 2006) (Figs. 2A, B).

At studied latitudes, the Central Andes holds several morphostructural provinces that from west to east, these are: The Coastal Cordillera in the forearc region, the high-standing Puna Plateau, the Eastern Cordillera, the Santa Bárbara System and the northern Pampean Ranges (Fig. 4). The general orogen structure at analyzed latitudes is dominated by a thick-skinned, and more locally hybrid deformation style, involving high-angle bivergent reverse faults in a thickened crust (e.g. Allmendinger et al., 1983; Hongn et al., 2010; Carrera and Muñoz, 2013; Martínez et al., 2020). The oldest deformation in this Andean segment has been dated as Late Cretaceous-Early Paleocene and produced basin inversion resulting in hybrid thrust belts and sedimentary basins in the inner forearc region (Arriagada et al., 2006; Martínez et al., 2017; 2018a; 2019; 2020; Bascuñán et al., 2019; López et al., 2019). In Cenozoic times the orogen expanded and propagated to the east in two possible ways: i) following a systematic and regular deformation pattern in an orogenic wedge style of propagation (e.g. Carrapa et al., 2005; Deeken et al., 2006; Carrapa and DeCelles, 2015) or ii) in a rather distributed or disparate propagation mode of deformation caused by a strong influence of the preexisting structural framework (e.g. Hongn et al., 2007; Strecker et al., 2012; del Papa et al., 2013; Montero-López et al., 2018; Payrola Bosio et al., 2019).

In this study, we focus on the southern Puna plateau which lies above the SPSS. The southern Puna region between 24°S and 28°S is separated from the northern Puna region by a major NW-trending structure known as the Olacapato–El Toro lineament (OTL) (Fig. 2B). The general structure of the Central Andean plateau in the Puna and the adjacent Eastern Cordillera morphostructural units, is related to steeply dipping, bivergent thrust faults rooted at >25 km depth into the crust (Allmendinger et al., 1997; Kley et al., 1999) (Fig. 4). The thick-skinned style of deformation in this segment has been explained by the presence of a structural framework linked to the Mesozoic Salta Rift that occupied the current Santa Barbara system, parts of Eastern Cordillera, and the Puna plateau (e.g., Kley et al., 1999) (Fig. 4). Shortening values in these fold and thrust belts yielded a minimum estimate of 142 km for the total magnitude of shortening at 24–25°S (Pearson et al., 2012).

The Cenozoic tectosedimentary history of the southern Puna plateau is relatively well understood. Regional studies revealed that south of the 25°S this area held a ~150 km wide Paleogene foreland basin that extended from the Salar de Antofalla region (B in Fig. 5) to the Sierra de Laguna Blanca (D in Fig. 5), indicating overall lithospheric flexure at this stage between ~40 and 28 Myr (Kraemer et al., 1999; Deeken et al., 2006; DeCelles et al., 2011; Sicks and Horton, 2011; Quade et al., 2015; Zhou et al., 2016a;b). This large flexural depocenter would have coexisted with intraplate contraction to east in the Eastern Cordillera (e.g. Coutand et al., 2001; Hongn et al., 2007; Del Papa et al., 2013; Zhou et al., 2016a;b; Montero-López et al., 2018) (Fig. 5). However, major orogenic development must have been located to the west as suggested by the presence of inner forearc thrust-belts (Arriagada et al., 2006; Martinez et al., 2020), the westward continental tilting reflected in the asymmetry of the Late Eocene-Early Oligocene flexural basin (Zhou et al., 2016a;b) and the existence of a ~4 km high topography in the western Puna border inferred from paleoaltimetry data (Canavan et al., 2014). This basin connected several late Eocene-early Oligocene synorogenic units that from west to east comprise the Quiñoas Formation, Antofagasta de la Sierra strata, and Pasto Ventura strata (Zhou et al., 2016b). The basin asymmetric geometry is inferred based on the presence of the thickest late Eocene-early Oligocene deposits (>3.4 km) in the western basin sector that diminish to the east to <0.5 km of sedimentary rocks bearing paleosol horizons, burrows and carbonate nodules indicating protracted subaerial exposure (Carrapa et al., 2005; Zhou et al., 2016a) (Fig. 5). A change in basin dynamics beginning as early as late Oligocene led to the compartmentalization of this broad flexural basin by several major basement cored uplift related to west and east-verging reverse faults forming small-scale flexural depocenters at the time the deformational front propagated eastwards up to the Late Miocene (e.g., Kraemer et al., 1999; Carrapa et al., 2005; Deeken et al., 2006; Zhou et al., 2014; Zhou and Schoenbohm, 2015; Zhou et al., 2016a;b) (Fig. 5). Basin fragmentation took place through exhumation of the Sierra de Calalaste (29-25 Myr, Carrapa et al., 2005; 25-20 Myr, Zhou et al., 2016b) (C in Fig. 5) and the Sierra Laguna Blanca (15–10 Myr, Zhou et al., 2014; Zhou and Schoenbohm, 2015) (D and G in Fig. 5). Exhumation of the southern Puna margin (F in Fig. 5) took place at a similar time between 25 and 15 Myr as indicated by apatite fission tracks data (Fig. 14; Carrapa et al., 2006). The latter is coincident with the proposal of the onset of internal orogenic drainage in the southern Puna from 24°S to 26°S between 24.2 and 15 Myr (Vandervoort et al., 1995; Coutand et al., 2001). Additional factors such as local lithospheric foundering in the plateau interior (Zhou and Schoenbohm, 2015) and oscillating basin infill and excavation linked to shifts of orographic precipitation (e.g., Sobel et al., 2003) may have regulated further uplift of localized basement-cored ranges in late Cenozoic times. By latest Miocene to Pliocene times contractional deformation reached the Santa Bárbara System and the Northern Pampean Ranges leading to basin inversion and basement block uplift, respectively (e.g. Carrapa et al., 2005; Deeken et al., 2006; Strecker et al., 2012; Carrapa and DeCelles, 2015; Zapata et al., 2019a,b) (the latter referred as H in Fig. 5).

Recently, Giambiagi et al. (2016) based on a regional paleostress analysis in the southern Puna proposed that between 13 and 8 Myr elevation and crustal thicknesses reached threshold values needed to generate the orogenic collapse in the hinterland region. To the east of the Central Andes, Cenozoic intraplate deformation has been first documented by Rossello (2007) and analyzed in detail by Peri (2012). This feature is associated with block uplift of Mesozoic and Cenozoic rocks of the Otumpa Hills located at about 950 km from the Chilean trench (Fig. 4). Interpretation of 2-D seismic lines indicates that initial deformation took place in the Paleozoic and attained its current expression during a reactivation episode linked to Andean orogeny in post-Eocene times (Peri, 2012). According to morphotectonic studies the Otumpa Hills are still active as indicated by recent drainage reorganizations in this area (Peri and Rossello, 2010).

The Late Oligocene to present contractional stage in the Puna region was accompanied by a significant crustal thickening from ~40-45 km to current values of ~60-70 km as inferred from La/Yb ratios from arc-related igneous rocks (Haschke et al., 2002; Kay et al., 1994, 2013) (Fig. 6). Notably, the significant crustal thickening in this orogenic sector is associated with relatively small amounts of shortening that does not overcome the 30% of the present crustal cross-section area (Kley and Monaldi, 1998; Pearson et al., 2012). Recent numerical modeling and geochemical studies indicate that the origin of the remaining crustal area is likely associated with along strike ductile lower crust flow leading to orogen inflation (Kay and Coira, 2009; Ouimet and Cook, 2010).

4.2. Spatial and temporal evolution of magmatism in the southern Puna plateau

In the last decades, several works have produced and compiled a significant amount of data of igneous rocks in the Central Andes in an effort to unravel crustal evolution and the geodynamics processes behind the central Andean magmatism (Scheuber and Reutter, 1992; Coira et al., 1993; Allmendinguer et al., 1997; Reuter et al., 2006; Trumbull et al., 2006; Mamani et al., 2010; DeCelles et al., 2015; Guzmán et al., 2014; Kay and Coira, 2009; Goss and Kay, 2009, among others). However, the spatio-temporal and compositional changes in arc rocks, as well as its relation to deformational events are still discussed (e.g., DeCelles et al., 2015; Kay et al., 2013). In this section, we focus on magmatism emplaced on the southern Puna plateau between 25°S and 27°30'S where the spatial, temporal and geochemical changes in igneous rocks are relatively well resolved. Extensive references to studies dealing with the geology, volcanology, and geochemistry of the southern Puna plateau and the arc region can be found in Kay et al. (1994), Kay and Coira (2009), Kay et al. (2013), and Guzmán et al. (2014).

The Mesozoic to early Paleogene arc constituted a narrow belt of ~50–100 km located at ~100-230 km from the trench that records a steady shifting to the east at about 1.5 km/Myr (e.g., Scheuber and Reutter, 1992) (Fig. 5). This arc migration has been explained by subduction erosion in the context of normal subduction (Trumbull et al., 2006). In the latest Paleogene times, at about 30 Ma, magmatic activity was significantly reduced for ~10 Ma to the south of 20°S (Kay and Coira, 2009; Trumbull et al., 2006). However, a more recent analysis of geochronological datasets shows that this interval of reduced magmatic activity was shorter, about 4 Ma from 30 to 26 Myr (Guzmán et al., 2015). To date, the origin of this reduced arc activity is still discussed (e.g., Coira et al., 1993; DeCelles et al., 2015; Kay and Coira, 2009). In the study area, Zhou et al. (2016a;b) associated this event to a low-flux stage related to the Cordilleran cycle (DeCelles et al., 2015). Between the latest Oligocene to Holocene, magmatic activity became volumetrically significant throughout the CVZ (Mamani et al., 2010; Trumbull et al., 2006). At analyzed latitudes, Neogene to recent arc rocks present an evolutionary trend towards enriched isotopic signatures, steeper REE patterns, and more crustal-like signatures likely resulting from interaction with a progressively thickened crust. This is well illustrated in the calc-alkaline medium to high-K2O andesitic to dacitic rocks of the Maricunga Belt (26–6 Myr) (Coira et al., 1993; Kay and Coira, 2009; Kay et al., 2013). In the 25–28°S segment, magmatism experienced an impressive broadening at ~26 Ma whose origin remains enigmatic (Allmendinger et al., 1997; Guzmán et al., 2014) (Fig. 5). Furthermore, Guzmán et al. (2014) noticed a coeval eastward arc front shifting based on the analysis of an extensive database constructed from their own field studies and a compilation of existing data (Trumbull et al., 2006; Pilger: http://www.pilger.us/id3.html, and CAGD: http://andes.gzg.geo.unigoettingen.de/). In fig. 6A we have corrected the spatiotemporal analysis of Guzmán et al. (2014) restituting the paleo-trench for 40 km of subduction erosion after 8 Ma (Goss and Kay, 2009). Noteworthy, these arc-to trench distances represent a minimum estimate as we did not take into account shortening in the upper-plate. Hence, arc migration and broadening magnitudes could have been larger. From 26 Ma onwards, the magmatism width varied with time, but it did not migrate substantially (Guzmán et al., 2014) (Figs. 5 and 6A). Contrarily, north of the southern Puna plateau between 12°S and 20°S, trenchward migration of magmatism has been described since ~24 Ma (Coira et al., 1993; Kay and Coira, 2009; Mamani e al., 2010) and since ~17 Ma at 20-23°S (Allmendinger et al.,1997; Reuter et al., 2006).

Kay and Coira (2009) through the analysis of the Neogene magmatic evolution between 24° and 28°S identified an additional eastward broadening of andesitic to dacitic stratovolcanoes, starting at 16 and enhancing at 8 Ma, and the production of voluminous ignimbrites from 6 to 2 Myr. These observations were interpreted as produced by a slab shallowing with subtle steepening at ~6 Ma, facilitating lithospheric delamination (Bianchi et al., 2013; Kay et al. (2013) (Fig. 6). Chemical and isotopic signatures of arc rocks erupted between ~28.2 and 26.7°S, present a particular trace element signature associated with variable heavy REE slopes (Sm/Yb=2–9), wt% Na2O (3–5.5), HFSE depletion (La/Ta=15–110) and Ba/La (15–55). This has been explained as produced by contaminants from the lower crust and source contamination in the mantle wedge by fluids resulting from melting of forearc material linked to the tectonic removal of ~40 km of forearc crust from 8 to 3 Myr (Goss and Kay, 2009; Kay and Coira, 2009; Kay et al., 2013). Coetaneous magmatic activity to the north emplaced in a thick arc crust north of 26.7°S have lower Sm/Yb (2–4) and La/Ta (15–45) ratios and wt% Na2O (3–4) than those to the south. A process of deep crustal flow in these rocks has been inferred based on a temporal trend towards more upper crustal-like trace element and isotopic signatures (Kay et al., 2013).

More recently, Guzmán et al. (2014) refined the Neogene magmatism dynamics and documented a southward migration of broadening arc activity between ~18 and 8 Myr. These authors indicate that the 25–26°S segment experienced maximum broadening in the 18–14.5 Myr interval; the 26–27°S segment in the 14.5–11.5 Myr interval; and the 27–28°S segment in the 11.5–8.3 Myr interval (Fig. 6A). Although still discussed, this migration has been related to the southward swept of the Juan Fernandez aseismic ridge that subducted obliquely at those times producing transient changes in the slab angle (Guzmán et al., 2014; Kay and Coira, 2009; Yañéz et al., 2001) (see current location on Fig. 2A).

To summarize, a reduced arc activity took place at ~30 Ma and was followed by a significant eastward arc migration and magmatic broadening in the 25–27°30’S segment of the CVZ is observed at ~26 Ma. From then onwards, the arc experienced local variations of transient character in width during middle to latest Miocene due to fluctuations in slab angle.

5. DISCUSSION

5.1. Geodynamic mechanism behind the spatio-temporal arc evolution

Spatiotemporal arc migrations and expansions have been mostly attributed to modifications in convergence rates, variations in slab dip, crustal thickening and absolute trench motion produced by subduction erosion or accretion (e.g., von Huene and Scholl, 1991; Kay et al., 2005; Haschke et al., 2002; Mamani et al., 2010; Karlstrom et al., 2014). Subduction erosion is expected to produce arc advance as the forearc area is reduced (e.g., von Huene and Scholl, 1991). The removed forearc crustal material may enter the mantle wedge contaminating the source of arc magmatism and hence, can be successfully tracked through the analysis of geochemical data (e.g. Stern, 1991; Kay et al., 2005). In the study area, the absence of significant source contamination in the mantle wedge at 26-18 Myr, inferred from isotopic data from arc rocks, indicates that subduction erosion was not a dominant process when the arc migrated (Kay et al., 2013). Arc shifting due to subduction erosion as well as those produced by alternative mechanisms such as crustal thickening (Karlstrom et al., 2014), are expected to produce a net arc migration but not necessarily an arc broadening as observed in the study area (Fig. 4, 5 and 6A).

Guzmán et al. (2014) analyzed the relationship between the arc dynamics in the study area and the convergence rate and found that these processes are poorly correlated. Indeed, most recent numerical modeling studies suggest that convergence controls arc-to-slab depth (England and Katz, 2010), but does not correlate well with the location of the melting region in arcs (Grove et al., 2009, 2010). More recent studies indicate that a trenchward arc expansion could be expected with increasing convergence rates (Karlstrom et al., 2014; Fig. 10a). If the latter is valid, taking into account the increment in convergence rates between ~26 and 25 Myr (Somoza, 1998), we would expect a trenchward arc migration and expansion at those times in the study area, which opposes the magmatic evolution followed in the southern Puna Plateau (Fig. 6A).

Additional factors such as upper crust structures may have influenced to a certain degree the location of the magmatic activity (e.g. Riller et al., 2006; Trumbull et al., 2006). This is well illustrated by the Neogene magmatic activity that followed NO-striking structures (Viramonte and Petrinovic, 1990; Coira et al., 1993; Matteini et al., 2002; Richards et al., 2006; among others). However; in some cases, the opposite could have also been true as several studies also indicate that thermomechanical weakening induced by magmatic intrusions tends to control the location of upper-crust structures (e.g. Ramos et al., 2002; Sagripanti et al., 2012).

Changes in slab dip are expected to control arc-trench distance as the mantle wedge is pushed-forward (Coney and Reynolds, 1977). Numerical modeling and the global analysis of subduction zones of Grove et al. (2009, 2010) show that changes in slab dip control arc width, causing narrowing or widening of magmatism, as well as net arc position causing forelandward or trenchward motion of the arc activity. The eastward frontal arc migration combined with eastward rear arc migration and the bulk arc broadening between ~30 and 26 Myr along with the change to a widespread upper-plate contraction and broken foreland formation is compatible with a progressive slab shallowing (Kay and Mpodozis, 2002, Ramos and Folguera, 2005; Schüte et al., 2010). More importantly, this hypothesis is the most compatible with the shallow subduction configuration currently observed beneath the study area and hence, most likely indicates the onset of the SPSS in the Late Oligocene.

5.2. Determination of potential paleo-slab angles

Two main methods are often applied to reconstruct paleo-slab angles. One approach is based on obtaining slab angles by assuming that the arc activity or its ancient bedrock record should intersect the top of the slab at a constant oceanic lithosphere dehydration depth around 100-150 km (e.g. Coney and Reynolds, 1997, Ramírez de Arellano, 2012). However, recent studies have shown that slab dehydration could be affected by plate kinematics such as variations in the convergence rate and hence, limiting this approach (England and Katz, 2010; Grove et al., 2009, 2010). The other methodology was mostly applied to the spatiotemporal magmatic evolution of several Andean segments (e.g. Kay and Abbruzzi, 1996; Kay and Copeland, 2006; Kay and Coira, 2009). It is based on the extrapolation of a current Wadati-Benioff zone and its associated arc-trench system to a neighboring area with a similar paleo-trench-arc distance and geochemical similarities. Below we use a different approach that considers a global subduction database of arc-trench distances and dip angles, which can be easily applied to reconstruct paleo-slab angles.

Fig. 7 shows the distribution of arc-trench distances and slab dips from Perrin et al. (2018), which is based on the global subduction zone compilation of Syracuse et al. (2010). This dataset base uses well-constrained slab geometries and is the most comprehensive compilation available. Similarly to previous studies (e.g. Jarrard, 1986; Syracuse and Abers, 2006; England et al., 2004), this diagram shows that arc-trench distance, D, correlates negatively with slab dip, δ. This diagram was originally built along 2-D numerical modeling to understand the thermal structure of the mantle wedge and its influence in arc location (Perrin et al., 2018). In this study, we take advantage of this diagram to track the potential evolution of slab dip though time by plotting the average D values from the three latitudinal segments analyzed in Fig. 6B (25-26°, 26-27°, and 27-28°) at 80-30 Myr, 26-18 Myr, 14-11 Myr, and 2.5 Ma arc stages. This analysis shows a subducting plate shallowing from dips of ~54° to ~16° that took place between 30 and 26 Myr and attained a minimum slab angle of ~7° at 14-11 Myr. Then, a subtle decrease to current values around 10° is observed associated with the SPSS (Fig. 7).

5.3. Linking the tectonomagmatic evolution of the southern Puna plateau with the SPSS

A new synthesis of the tectonomagmatic history of the southern Puna plateau sheds light on the onset of the SPSS and its relation to the southern Puna plateau tectonics. The observation of migration and broadening of the magmatic activity at ~26 Ma from a former westward arc position likely indicates that the SPSS began to develop since the Late Oligocene (Figs. 5 and 6A). This process was preceded by ~4 Ma of reduced magmatic activity that may indeed indicate the onset of the reconfiguration of the slab angle at ~30 Ma. At this time, a large Eocene-early Oligocene flexural basin located south the 25°S (Zhou et al., 2017) was compartmentalized by the distributed growth of basement-cored structures lasting up to Miocene times (Kraemer et al., 1999; Carrapa et al., 2005; Deeken et al., 2006; Zhou et al., 2016a;b) (Fig. 5). Also, during this same period, the forearc region experienced a reactivation in the fold and thrust belts preserved in Oligocene to Miocene syn-kinematic sequences described in 2-D seismic reflection lines (Martínez et al., 2019; 2020). In addition, after Eocene times intraplate deformation took place at ~950 km from the trench causing surface uplift of the Otumpa intraplate Hills (Rossello, 2007, Peri, 2012)

(Fig. 4). Although this deformation style is not unique to flat/shallow subduction zones (e.g. Kley et al., 1999; Gianni et al., 2017), we suggest that distributed deformation and intraplate deformation likely resulted from an increased interplate coupling as expected in these geodynamic settings and as documented in several recent and ancient shallow and flat-slab settings (Dickingson and Snyder, 1978; Jordan and Allmendinger, 1986; Gianni et al., 2018a,b) (Figs. 1 and 8). At this moment, an applied end load stress favored by a higher plate coupling would have triggered stress propagation through the plate margin lithosphere, spatially concentrating deformation along inherited plate weaknesses (Kley et al., 1999; Weil et al., 2014; Zhou et al., 2016a; Axen et al., 2018). In Miocene-Pliocene times, further changes in the slab angle, produced local variations in arc width and upper plate contraction in the Santa Barbara and Northern Pampean ranges (Carrapa et al., 2005; Deeken et al., 2006; Kay and Coira, 2009; Zapata et al., 2019a,b). Also at this time, the influence of transverse lineaments in magmatic location appears to be stronger (Trumbull et al., 2006). We suggest that as the high plate coupling triggered distal stress propagation, the eastward migration of the magmatic activity provided the most favorable conditions for significant the basement cored deformation in the plate margin sector. This is because under intense magmatic activity the initial thermomechanical conditions of the lithosphere are modified and tectonic reactivations and new faulting are more easily produced (e.g. Ramos et al., 2002; Martinez et al., 2018b).

The numerical simulations of Ouimet and Cook (2014) indicate that late Cenozoic Andean orogen-parallel crustal flow did not penetrate into the cold regions of stronger lower crust above the Chilean and Peruvian flat-slab segments (Fig. 1). In the study area, the Chilean flat-slab blocked this southward flow and inflated the lower crust beneath the Puna plateau. In this context, the SPSS must have allowed the existence of a mantle wedge and a hot upper-plate, as currently seen (Mulcahy et al., 2014) favoring orogen-parallel crustal flow.

The progressive upper plate contraction linked to slab shallowing acted in concert with the lower crustal flow to thicken the crust up to 60-70 km driving lower lithosphere delamination at ~6-4 Myr (Bianchi et al., 2013; Kay et al., 2013) (Figs. 6B and 8). Kay and Coira (2009) indicated that the lithospheric delamination took place after a slab steepening. However, despite the relatively steeper slab beneath the Cerro Galán caldera (CGC, in Fig. 2B) respect to the Chilean flat-subduction in the south (Fig. 10; Mulcahy et al., 2014), the existence of the SPSS, suggests that this process took place under an essentially shallow angle configuration to the west. In this context, delamination would have been allowed only after a slight steepening of the easternmost slab sector (Fig. 6 and 8). A similar example of syn-convergent delamination during shallow subduction has been proposed for the early stages of the Late Neogene-Pliocene Peruvian flat-slab (Coldwell et al., 2011).

Although the Andes began its uplift in Early Late Cretaceous times, the most significant deformation took place during the Paleogene and Neogene. At this time, changes in several geodynamic processes such as upper-plate velocity (Silver et al., 1998), slab age, subduction length and depth (e.g. Capitanio et al., 2011; Faccena et al., 2017) as well as the onset of critical climatic conditions (e.g. Lamb and Davis, 2003) acted in concert to trigger plate margin-scale contraction and crustal thickening. Our observations do not preclude the role of these first-order tectonic factors in the tectonic evolution of the study area. However, the close relationship between the evolution of the southern Puna plateau and the onset of shallow subduction lead us to conclude that the development of the SPSS was a key geodynamic process in the last building stages of this region of the Central Andes. This process would have acted as an enhancement factor in Andean orogenesis at studied latitudes contributing to the formation of one of the thickest orogenic crust on Earth.

Commonly invoked causes for shallow or flat-subduction are highly diverse including i) subduction of thickened and buoyant oceanic crust such as oceanic plateaus or aseismic ridges (e.g. Gutcher et al., 2000), ii) hydrodynamic suction due to the presence of a thick cratonic keel (~200 km) next to the active margin (Manea et al., 2012) or iii) a low asthenosphere viscosity (Manea and Gurnis, 2007), and overriding of an old and slowly retreating slab (Schellart, 2020). More recent studies indicate that the most favorable conditions for full flat-slab development are met when several of these factors act in concert (Hu et al., 2016).

Potential candidates for triggers of the SPSS are the Taltal and Copiapo aseismic ridges currently subducting west of the study area (Fig. 2A). However, their timing of interaction with the trench at ~10 Ma (Bello-Gonzalez et al., 2018) does not correlate with the onset of the SPSS in Oligocene times precluding any influence in the onset of shallow subduction in the southern Puna plateau. Moreover, the effect of aseismic ridge subduction as a driving mechanism for Andean flat-slabs has been disregarded based on recent kinematic reconstructions (Skinner and Clayton, 2013). Also, 2-D numerical modeling studies indicate that the buoyant lithosphere is not sufficient to yield a shallow subduction configuration (e.g. Gerya et al., 2009). However, at least the Copiapo ridge is suggested to have acted as a lower plate asperity that influenced the pattern of upper plate deformation at 27°S (Álvarez et al., 2015).

The lack of a sufficiently deep lithosphere (~200 km) next to the Puna plateau enhancing slab hydrodynamic suction hampers invoking this mechanism for the development of the SPSS. Alternatively, it could be argued that shallow subduction beneath the southern Puna plateau is somewhat sustained or influenced by the Chilean flat-slab to the south between 27º30'and 33ºS (Fig. 2A). However, the fact that the main arc migration in the study area took place much earlier than the one related to the development of the Chilean flat-slab (~18 Ma, Ramos et al., 2002) makes this possibility untenable. Between ~26 and 20 Myr, the region occupied by the Chilean flat-slab was under extension related to a steeply dipping slab (Coira et al., 1993, ay et al., 2013; Winocur et al., 2015; Jones et al., 2016). Moreover, if the Chilean flat-slab can indeed influence subduction angles far from its location we would expect a similar shallowly dipping transition to the south of this flat-slab, which strongly contrast with the normal slab angle described in that area (Cahill and Isacks, 1992; Mulcahy et al., 2014). Alternatively, we suggest that the change in the subduction angle in the SPSS since Late Oligocene times could have occurred from local changes in the viscosity of the mantle wedge. Depth-dependent slab dehydration transports fluids into the mantle wedge where the viscosity is decreased. Numerical models show that in cases of increased fluid-flux such a decrease in viscosity could form a low viscosity wedge that enhances suction in the mantle wedge inducing slab shallowing (Manea and Gurnis, 2007). These models predict that there could be a larger volatile input into the wedge when arcs migrate toward the trench, which is compatible with the progressive slab fluid contents inferred for the southern Puna Magmatism (Kay et al., 2013) and the suggestion of a hotter asthenospheric wedge based on seismology surveys (Mulcahy et al., 2014). However, the reason why this mantle wedge obtained these characteristics is puzzling. Therefore, further studies are necessary to assess the origin of the SPSS.

6. CONCLUSION

The analysis of subduction zone profiles indicates that the Nazca plate beneath the southern Puna plateau is characterized by a ~200 km wide shallow portion at a depth of ~100-120 km that dips 10-12°E at 300 km from the trench. In general, this slab segment is between ~30 and 90 km shallower than the rest of the slab beneath the CVZ. A new synthesis of the tectonomagmatic record in this region indicates that changes in slab angle began in the late Oligocene times, as revealed by an eastward arc-front migration and magmatic broadening that took place at ~26 Ma. This process was preceded by ~4 Ma of reduced arc activity that we relate to the onset of the subduction reconfiguration. A new approach based on the application of an arc-trench distance vs. slab dip diagram including global subduction zone dataset shows that slab shallowing took place progressively changing from ~54° to ~16° between ~30 and 26 Myr. The slab attained minimum values of 7° at 14 Ma and steepened subtly afterward to the current SPSS angle of ~10°, consistent with the proposal of a slab steepening between 6-3 Myr (Kay and Coira, 2009). We encourage the use of this straightforward methodology to extract paleo-angles from the bedrock record in future studies dealing with similar problems. We envision that an applied end load favored by an increased interplate coupling resulting from slab shallowing would have triggered a significant crustal thickening and the destruction of a pre-existing Eocene-early Oligocene foreland basin south of 25°S (Zhou et al., 2017). An effective stress transmission linked to the SPSS would have caused the enigmatic late Cenozoic surface uplift of the Otumpa Hills at ~950 km from the trench similar to intraplate deformation in other shallow/flat subduction settings. The close link between the evolution of the southern Puna plateau and the onset of shallow subduction lead us to conclude that this geodynamic process was a key factor prompting mountain-building in this region. This process likely acted jointly with major changes in plate kinematic and climatic conditions in the Cenozoic enhancing Andean orogenesis at studied latitudes. In general, our observations do not contradict previous studies mostly concentrated in the post-18 Ma evolution of this area (e.g. Kay and Coira, 2009; Kay et al., 2013) but integrate them into a larger geodynamic evolution that began earlier than previously acknowledge. The tectonic role of the SPSS was probably overlooked and obscured by the formation of the predominant Chilean flat-subduction to the south since ~16 Ma that captured the attention of most studies dealing with subduction geometry and its link with magmatism and deformation.

7. ACKNOWLEDGEMENTS

This study was supported by the Consejo Nacional de Investigaciones Científicas y Técnicas (CONICET). This study benefited greatly from the comments of Dr. Fernando Martínez and two anonimous reviewers. We are greatful to the editor Dr. Ramón Carbonell for effective handling of the manuscript and Dr. Lucas Fennell for providing insightful comments on a preliminary version of this manuscript.

8. REFERENCES

Allmendinger, R. W., Ramos, V. A., Jordan, T. E., Palma, M., & Isacks, B. L. (1983). Paleogeography and Andean structural geometry, northwest Argentina. Tectonics, 2(1), 1-16.

Arriagada, C., Cobbold, P.R., Roperch, P., 2006. The Salar de Atacama basin: a record of compressional tectonics in the Central Andes since mid-Cretaceous. Tectonics 25. https://doi.org/10.1029/2004TC001770.

Allmendinger, R.W., Jordan, T.E., Kay, S.M., Isacks, B.L., 1997. The evolution of the Altiplano-Puna plateau of the Central Andes. Annual Review of Earth and Planetary Sciences 25, 139-174. doi:10.1146/annurev.earth.25.1.139.

Álvarez, O., Gimenez, M., Folguera, A., Spagnotto, S., Bustos, E., Baez, W., Braitenberg, C., 2015. New evidence about the subduction of the Copiapó ridge beneath South America, and its connection with the Chilean-Chilean flat slab, tracked by satellite GOCE and EGM2008 models. Journal of Geodynamics 91, 65-88.

Axen, G. J., van Wijk, J. W., & Currie, C. A. (2018). Basal continental mantle lithosphere displaced by flat-slab subduction. Nature Geoscience, 11(12), 961.

Barazangi, M., Isacks B.L., 1976. Spatial distribution of earthquakes and subduction of the nazca plate beneath South America. Geology 4, 686-692.

Bascuñán, S., Maksymowicz, A., Martinez, F., Becerra, J., Arriagada, C., Deckart, K., 2019. Geometry and late Mesozoic-Cenozoic evolution of the Salar de Atacama Basin (22°30′ -24°30′ S) in the northern Central Andes: new constraints from geophysical, geochronological and field data. Tectonophysics 759. https://doi.org/10.1016/j. tecto.2019.04.008.

Bello-González, J. P., Contreras-Reyes, E., & Arriagada, C. (2018). Predicted path for hotspot tracks off South America since Paleocene times: Tectonic implications of ridge-trench collision along the Andean margin. Gondwana Research, 64, 216-234.

Bianchi, M., Heit, B., Jakovlev, A., Yuan, X., Kay, S., Sandvol, E., Alonso, R., Coira, B., Brown, L., Kind, R., et al., 2013. Teleseismic tomography of the southern Puna plateau in Argentina and adjacent regions. Tectonophysics 586, 65-83. doi:10.1016/j.tecto.2012.11.016.

Cahill, T., Isacks, B.L., 1992. Seismicity and shape of the subducted Nazca plate. Journal of Geophysical Research 97, 17503. doi:10.1029/92jb00493.

Caminos, R. L., & González, P. D. (1997). Mapa geológico de la República Argentina.

Canavan RR and 5 coauthors (2014) Early Cenozoic uplift of the Puna Plateau, Central Andes, based on stable isotope paleoaltimetry of hydrated volcanic glass. Geology 42: 447-450

Calixto, F.J., Robinson, D., Sandvol, E., Kay, S., Abt, D., Fischer, K., Heit, B., Yuan, X., Comte, D., Alvarado, P., 2014. Shear wave splitting and shear wave splitting tomography of the southern Puna plateau. Geophysical Journal International 199, 688-699. doi:10.1093/gji/ggu296.

Capitanio, F.A., Faccenna, C., Zlotnik, S., Stegman, D.R., 2011. Subduction dynamics and the origin of Andean orogeny and the Bolivian orocline. Nature 480, 83–86. http://dx.doi.org/10.1038/nature10596.

Carrapa, B., Adelmann, D., Hilley, G.E., Mortimer, E., Sobel, E.R., Strecker, M.R., 2005. Oligocene range uplift and development of plateau morphology in the Southern Central Andes. Tectonics 24. doi:10.1029/2004tc001762.

Carrapa, B., Strecker, M., Sobel, E., 2006. Cenozoic orogenic growth in the Central Andes: Evidence from sedimentary rock provenance and apatite fission track thermochronology in the Fiambalá basin, southernmost puna plateau margin (NW Argentina). Earth and Planetary Science Letters 247, 82-100. doi:10.1016/j.epsl.2006.04.010.

Carrapa, B., & DeCelles, P. G. (2015). Regional exhumation and kinematic history of the central Andes in response to cyclical orogenic processes. Geol. Soc. Am. Mem, 212, 201-213.

Carrera, N., & Muñoz, J. A. (2013). Thick-skinned tectonic style resulting from the inversion of previous structures in the southern Cordillera Oriental (NW Argentine Andes). Geological Society, London, Special Publications, 377(1), 77-100.

Coira, B., Kay, S. M., & Viramonte, J. (1993). Upper Cenozoic magmatic evolution of the Argentine Puna—A model for changing subduction geometry. International Geology Review, 35(8), 677-720.

Coney, P,J., Reynolds, S.J., 1977. Cordilleran benioff zones. Nature, 270(5636), 403.

Coldwell, B., Clemens, J., & Petford, N. (2011). Deep crustal melting in the Peruvian Andes: felsic magma generation during delamination and uplift. Lithos, 125(1-2), 272-286.

Coutand, I., Cobbold, P.R., de Urreizieta, M., Gautier, P., Chauvin, A., Gapais, D., Rosello, E.A., and López-Gamundi, O., 2001, Style and history of Andean deformation, Puna plateau, northwestern Argentina: Tectonics, v. 20, p. 210–234, doi:10.1029/2000TC900031.

DeCelles, P.G., Carrapa, B., Horton, B.K., Gehrels, G.E., 2011. Cenozoic foreland basin system in the central Andes of northwestern Argentina: implications for An-dean geodynamics and modes of deformation. Tectonics30. http://dx.doi.org/10.1029/2011TC002948.

DeCelles, P., Zandt, G., Beck, S., Currie, C., Ducea, M., Kapp, P., Gehrels, G., Carrapa, B., Quade, J., Schoenbohm, L., 2015. Cyclical orogenic processes in the Cenozoic Central Andes. Geological Society of America Memoirs 212, MWR212-22.

Deeken, A., Sobel, E. R., Coutand, I., Haschke, M., Riller, U., & Strecker, M. R. (2006). Development of the southern Eastern Cordillera, NW Argentina, constrained by apatite fission track thermochronology: From early Cretaceous extension to middle Miocene shortening. Tectonics, 25(6).

Del Papa, C., Hongn, F., Powell, J., Payrola, P., Do Campo, M., Strecker, M. R., ... I. Petrinovic, A. K. Schmitt & Pereyra, R. (2013). Middle Eocene-Oligocene broken-foreland evolution in the Andean Calchaqui Valley, NWArgentina: insights fromstratigraphic, structural and provenance studies. Basin Research, 25(5), 574-593.

Dickinson, W.R., Snyder, W.S., 1978. Plate tectonics of the Laramide orogeny. Geol. Soc. Am. Mem. 151, 355–366.

England, P., Engdahl, R., Thatcher, W., 2004. Systematic variation in the depths of slabs beneath arc volcanoes. Geophys. J. Int.156 (2), 377–408.

England, P. C., & Katz, R. F. (2010). Melting above the anhydrous solidus controls the location of volcanic arcs. Nature, 467(7316), 700.

Faccenna, C., Oncken, O., Holt, A. F., Becker, T. W., 2017. Initiation of the Andean orogeny by lower mantle subduction. Earth Planet. Sci. Let. 463, 189-201.

Folguera, A., Ramos, V.A., 2011. Repeated eastward shifts of arc magmatism in the Southern Andes: a revision to the long-term, pattern of Andean uplift and magmatism. J. South Am. Earth Sci. doi:10.1016/j.jsames.2011.04.003.

Giambiagi, L., Alvarez, P., Spagnotto, S., 2016. Temporal variation of the stress field during the construction of the Central Andes: Constrains from the volcanic arc region (22-26°S), western cordillera, Chile, during the last 20Ma. Tectonics 35, 2014-2033. doi:10.1002/2016tc004201.

Gianni, G. M., Echaurren, A., Folguera, A., Likerman, J., Encinas, A., Garcia, H. P. A., Dal Molin, C., & Valencia, V. A. (2017). Cenozoic intraplate tectonics in Central Patagonia: Record of main Andean phases in a weak upper plate. Tectonophysics, 721, 151-166.

Gianni, G. M., Dávila, F. M., Echaurren, A., Fennell, L., Tobal, J., Navarrete, C., Folguera. A. & Giménez, M. (2018a). A geodynamic model linking Cretaceous orogeny, arc migration, foreland dynamic subsidence and marine ingression in southern South America. Earth-Science Reviews, 185, 437-462.

Gianni, G. M., Navarrete, C., Liendo, I., Díaz, M., Giménez, M. E., Encinas, A., & Folguera, A. (2018b). Cretaceous intraplate contraction in southern Patagonia: a far- field response to changing subduction dynamics?. Tectonics, 37(9), 2915-2937.

Goss, A. R. & Kay, S. M. 2009. Extreme high field strength element (HFSE) depletion and near-chondritic Nb/Ta ratios in Central Andean adakite-like lavas (~27°S, ~68°W). Earth and Planetary Science Letters, 270, 97–109.

Grove, T., Till, C., Lev, E., Chatterjee, N., Medard, E., 2009. Kinematic variables and water transport control the formation and location of arc volcanoes. Nature, 459, 694–697 (2009); erratum 460, 1044 (2009)

Grove, T.L., Till, C.B., Lev, E., Chatterjee, N., Medard, E., 2010. Global systematics of arc volcano position, Grove et al. reply. Nature, 468:E7–8

Gutscher, M.A., Spakman, W., Bijwaard, H., Engdahl, E.R., 2000. Geodynamic of flat subduction: seismicity and tomographic constraints from the Andean margin. Tectonics, 19, 814–833

Gutscher, M. A., & Peacock, S. M. (2003). Thermal models of flat subduction and the rupture zone of great subduction earthquakes. Journal of Geophysical Research: Solid Earth, 108(B1), ESE-2.

Guzmán, S., Grosse, P., Montero-López, C., Hongn, F., Pilger, R., Petrinovic, I., Seggiaro, R. & Aramayo, A., 2014. Spatial–temporal distribution of explosive volcanism in the 25–28 S segment of the Andean Central Volcanic Zone. Tectonophysics 636, 170-189.

Haschke, M. R., Scheuber, E., Günther, A., & Reutter, K. J. (2002). Evolutionary cycles during the Andean orogeny: repeated slab breakoff and flat subduction?. Terra nova, 14(1), 49-55.

Hayes, G. P., Moore, G. L., Portner, D. E., Hearne, M., Flamme, H., Furtney, M., & Smoczyk, G. M. (2018). Slab2, a comprehensive subduction zone geometry model. Science, 362(6410), 58-61.

Hongn, F., Papa, C. D., Powell, J., Petrinovic, I., Mon, R., & Deraco, V. (2007). Middle Eocene deformation and sedimentation in the Puna-Eastern Cordillera transition (23-26 S): Control by preexisting heterogeneities on the pattern of initial Andean shortening. Geology, 35(3), 271-274.

Hongn, F., Mon, R., Petrinovic, I., Del Papa, C., & Powell, J. (2010). Inversión y reactivación tectónicas Cretácico-Cenozoicas en el noroeste Argentino: Influencia de las heterogeneidades del basamento Neoproterozoico-Paleozoico inferior. Revista de la Asociación Geológica Argentina, 66(1), 38-53.

Hu, J., Liu, L., Hermosillo, A., & Zhou, Q., 2016. Simulation of late Cenozoic South American flat-slab subduction using geodynamic models with data assimilation. Earth and Planetary Science Letters 438, 1-13.

Jarrard, R.D., 1986, Relations among subduction parameters: Reviews of Geophysics, v. 24, p. 217–284, doi: 10.1029/RG024i002p00217.

Jones, R. E., Kirstein, L. A., Kasemann, S. A., Litvak, V. D., Poma, S., Alonso, R. N., & Hinton, R. (2016). The role of changing geodynamics in the progressive contamination of

Late Cretaceous to Late Miocene arc magmas in the southern Central Andes. Lithos, 262, 169-191.

Jordan, T. E., and Allmendinger, R. W. (1986). The Sierras Pampeanas of Argentina; a modern analogue of Rocky Mountain foreland deformation. American Journal of Science, 286(10), 737-764.

Karlstrom, L., Lee, C.T., Manga, M., 2014. The role of magmatically driven lithospheric thickening on arc front migration. Geoch. Geophy. Geosyst. 15(6), 2655-2675.

Kay, S. M., Mpodozis, C., Tittler, A., & Cornejo, P. (1994). Tertiary magmatic evolution of the Maricunga mineral belt in Chile. International Geology Review, 36(12), 1079-1112.

Kay, S. M., & Abbruzzi, J. M. (1996). Magmatic evidence for Neogene lithospheric evolution of the. Tectonophysics, 259, 15-28.

Kay, S.M., Mpodozis, C., 2002. Magmatism as a probe to the Neogene shallowing of the Nazca plate beneath the modern Chilean flat-slab. Journal of South American Earth Sciences 15, 39–57.

Kay, S.M., Godoy, E., Kurtz, A., 2005. Episodic arc migration, crustal thickening, subduction erosion, and magmatism in the south-central Andes: Geological Society of America Bulletin, v. 117, p. 67–88, doi: 10.1130/B25431.1.

Kay, S.M., Copeland, P., 2006. Early to middle Miocene backarc magmas of the Neuquén basin: Geochemical consequences of slab shallowing and the westward drift of South America. In: Kay, S.M., Ramos, V.A. (Eds.), Late Cretaceous to Recent magmatism and tectonism of the Southern Andean margin at the latitude of the Neuquen basin (36-39ºS). Geol Soc. Am. Special Paper 407, pp. 185-214.

Kay, S.M., Coira, B.L., 2009. Shallowing and steepening subduction zones, continental lithospheric loss, magmatism, and crustal flow under the Central andean Altiplano-Puna plateau. Geological Society of America Memoirs 204, 229-259.

Kay, S.M., Mpodozis, C., Gardeweg, M., 2013. Magma sources and tectonic setting of Central Andean andesites (25.5-28°S) related to crustal thickening, forearc subduction erosion and delamination. Geological Society, London, Special Publications 385, 303-334. doi:10.1144/sp385.11.

Kley, J., & Monaldi, C. R. (1998). Tectonic shortening and crustal thickness in the Central Andes: How good is the correlation?. Geology, 26(8), 723-726.

Kley, J., Monaldi, C., Salfity, J., 1999. Along-strike segmentation of the Andean foreland: causes and consequences. Tectonophysics 301(1-2), 75-94.

Kraemer, B., Adelmann, D., Alten, M., Schnurr, W., Erpenstein, K., Kiefer, E., Van Den Bogaard, P., Go, K., 1999. Incorporation of the Paleogene foreland into the Neo-gene Puna plateau: The Salar de Antofalla area, NW Argentina. J. South Am. Earth Sci.12.

Mamani, M., Worner, G., Sempere, T., 2010. Geochemical variations in igneous rocks of the central andean orocline (13°S to 18°S): Tracing crustal thickening and magma generation through time and space. Geological Society of America Bulletin 122, 162-182. doi:10.1130/b26538.1.

Manea, V., & Gurnis, M. (2007). Subduction zone evolution and low viscosity wedges and channels. Earth and Planetary Science Letters, 264(1-2), 22-45.

Manea, V. C., Manea, M., Ferrari, L., Orozco-Esquivel, T., Valenzuela, R. W., Husker, A., & Kostoglodov, V. (2017). A review of the geodynamic evolution of flat slab subduction in Mexico, Peru, and Chile. Tectonophysics, 695, 27-52.

Martínez, F., Arriagada, C., Pena, M., Del Real, I., Deckart, K., 2013. The structure of the Chanarcillo Basin: an example of tectonic inversion in the Atacama region, northern Chile. J. South Am. Earth Sci. 42, 1–16.

Martínez, F., González, R., Bascuñan, S., Arriagada, C., 2017. Structural styles of the salar de Punta Negra basin in the preandean depression (24°-25°S) of the central Andes. J. South Am. Earth Sci. https://doi.org/10.1016/j.jsames.2017.08.004.

Martínez, F., López, C., Bascuñan, S., Arriagada, C., 2018a. Tectonic interaction between Mesozoic to Cenozoic extensional and contractional structures in the Pre-andean Depression (23°–25° S): geologic implications for the central Andes. Tectonophysics 744, 333–349.

Martínez, F., Montanari, D., Del Ventisette, C., Bonini, M., & Corti, G. (2018b). Basin inversion and magma migration and emplacement: Insights from basins of northern Chile. Journal of Structural Geology, 114, 310-319.

Martínez, F., Kania, J., Muñoz, B., Riquelme, R., & López, C. (2020). Geometry and development of a hybrid thrust belt in an inner forearc setting: Insights from the Potrerillos Belt in the Central Andes, northern Chile. Journal of South American Earth Sciences, 98, 102439.

Martinod, J., Husson, L., Roperch, P., Guillaume, B., & Espurt, N. (2010). Horizontal subduction zones, convergence velocity and the building of the Andes. Earth and Planetary Science Letters, 299(3), 299-309.

Matteini, M., R. Mazzuoli, R. Omarini, R. A. F. Cas, and R. Maas (2002), Geodynamical evolution of the Central Andes at 24°S as inferred by magma composition along the Calama–Olacapato–El Toro transversal volcanic belt, J. Volcanol. Geotherm. Res., 118, 205–228, doi:10.1016/ S0377-0273(02)00257-3.

Montero-López, C., del Papa, C., Hongn, F., Strecker, M. R., & Aramayo, A. (2018). Synsedimentary broken-foreland tectonics during the Paleogene in the Andes of NW Argentine: new evidence from regional to centimeter-scale deformation features. Basin Research 2016, 1-18. doi 10.1111/bre.12212

Mulcahy, P., Chen, C., Kay, S.M., Brown, L.D., Isacks, B.L., Sandvol, E., Heit, B., Yuan, X., Coira, B.L., 2014. Central Andean mantle and crustal seismicity beneath the southern Puna plateau and the northern margin of the Chilean-Chilean flat slab. Tectonics 33, 1636-1658. doi:10.1002/2013tc003393.

Lamb, S., & Davis, P. (2003). Cenozoic climate change as a possible cause for the rise of the Andes. Nature, 425(6960), 792.

Lallemand, S., Heuret, A., and Boutelier, D., 2005, On the relationship between slab dip, back-arc stress, upper plate absolute motion, and crustal nature in subduction zones: Geochemistry, Geophysics, Geosystems, v. 6, Q09006, doi: 10.1029/2005GC000917.

López, C., Martínez, F., Maksymowicz, A., Giambiagi, L., Riquelme, R., 2019. What is the structure of the forearc region in the Central Andes of northern Chile? An approach from field data and 2-D reflection seismic data. Tectonophysics. https://doi.org/10.1016/j.tecto.2019.228187.

Oncken, O., Hindle, D., Kley, J., Elger, K., Victor, P., Schemmann, K., 2006. Deformation of the Central Andean upper plate system-Facts, fiction, and constraints for plateau models, in: The Andes. Springer, pp. 3-27.

Orts, D.L., Folguera, A., Encinas, A., Ramos, M., Tobal, J., Ramos, V.A. 2012b. Tectonic development of the North Patagonian Andes and their related Miocene foreland basin (41°30′–43° S). Tectonics, 31, 1–24.

Ouimet, W. B., & Cook, K. L. (2010). Building the central Andes through axial lower crustal flow. Tectonics, 29(3).

Pearson, D. M., Kapp, P., DeCelles, P. G., Reiners, P. W., Gehrels, G. E., Ducea, M. N., & Pullen, A. (2013). Influence of pre-Andean crustal structure on Cenozoic thrust belt kinematics and shortening magnitude: Northwestern Argentina. Geosphere, 9(6), 1766-1782.

Peri, V. G. (2012). Caracterización morfotectónica de las Lomadas de Otumpa (Gran Chaco, Santiago del Estero y Chaco): influencias en el control del drenaje (Doctoral dissertation, Facultad de Ciencias Exactas y Naturales. Universidad de Buenos Aires).

Peri, V. G. (2012). Caracterización morfotectónica de las Lomadas de Otumpa (Gran Chaco, Santiago del Estero y Chaco): influencias en el control del drenaje (Doctoral dissertation, Facultad de Ciencias Exactas y Naturales. Universidad de Buenos Aires).

Peri, VG & EA Rossello. 2010. Anomalías morfoestructurales del drenaje del Río Salado sobre las lomadas de Otumpa (Santiago del Estero y Chaco) detectadas por procesamiento digital. Revista de la Asociación Geológica Argentina 66(4): 634-645.

Perrin, A., Goes, S., Prytulak, J., Rondenay, S., & Davies, D. R. (2018). Mantle wedge temperatures and their potential relation to volcanic arc location. Earth and Planetary Science Letters, 501, 67-77.

Quade, J., Dettinger, M. P., Carrapa, B., DeCelles, P., Murray, K. E., Huntington, K. W., A. Cartwrigh, R.R. Canavan, G. Gehrels & Clementz, M. (2015). The growth of the central Andes, 22 S–26 S. Geol Soc Am Mem, 12, 277-308.

Ramírez de Arellano, C., Putlitz, B., Müntener, O., & Ovtcharova, M. (2012). High precision U/Pb zircon dating of the Chaltén Plutonic Complex (Cerro Fitz Roy, Patagonia) and its relationship to arc migration in the southernmost Andes. Tectonics, 31(4).

Ramos, V. A., Cristallini, E. O., & Pérez, D. J. (2002). The Pampean flat-slab of the Central Andes. Journal of South American earth sciences, 15(1), 59-78.

Ramos, V.A., Folguera, A., 2005. Tectonic evolution of the Andes of Neuquén: constraints derived from the magmatic arc and foreland deformation. In: Veiga, G.D., Spalletti, L.A., Howell, J.A., Schwarz, E. (Eds.), The Neuquén Basin, Argentina: A case Study in Sequence Stratigraphy and Basin Dynamics Geol. Soc. Lond., Special Publications, 252:15-35

Ramos, V.A., Folguera, A., 2009. Andean flat-slab subduction through time. Geological Society, London, Special Publications 327, 31-54. doi:10.1144/sp327.3.

Ramos, V. A., Litvak, V. D., Folguera, A., & Spagnuolo, M. (2014). An Andean tectonic cycle: From crustal thickening to extension in a thin crust (34–37 SL). Geoscience Frontiers, 5(3), 351-367.

Reutter, K. J., Charrier, R., Götze, H. J., Schurr, B., Wigger, P., Scheuber, E., Giese, P., Reuther, C-D., Schmidt, S., Rietbrock, A., & Chong, G. (2006). The Salar de Atacama Basin: a subsiding block within the western edge of the Altiplano-Puna Plateau. In The Andes (pp. 303-325). Springer, Berlin, Heidelberg.

Richards, J. P., Ullrich, T., & Kerrich, R. (2006). The late Miocene–Quaternary Antofalla volcanic complex, southern Puna, NW Argentina: protracted history, diverse petrology, and economic potential. Journal of Volcanology and Geothermal Research, 152(3-4), 197-239.

Riller, U., Götze, H. J., Schmidt, S., Trumbull, R. B., Hongn, F., & Petrinovic, I. A. (2006). Upper-crustal structure of the Central Andes inferred from dip curvature analysis of isostatic residual gravity. In The Andes (pp. 327-336). Springer, Berlin, Heidelberg.

Rossello, E.A., Bordarampé, C.P. y Peri, V.G. 2007. The Otumpa faulting (Gran Chaco plain, Argentina): the farthest megastructure due to the Central Andean flat slab subduction. Subduction Zone Geodynamics Conference (Montpellier), Mémoires Géosciences-Montpellier 41: 62.

Sagripanti, L., Vera, E. A. R., Gianni, G. M., Folguera, A., Harvey, J. E., Farías, M., & Ramos, V. A. (2015). Neotectonic reactivation of the western section of the Malargüe fold and thrust belt (Tromen volcanic plateau, Southern Central Andes). Geomorphology, 232, 164-181.

Sánchez, M. A., Ariza, J. P., García, H. P., Gianni, G. M., Weidmann, M. C., Folguera, A., Federico Lince Kliner & Martinez, M. P. (2018). Thermo-mechanical analysis of the Andean lithosphere over the Chilean-Pampean flat-slab region. Journal of South American Earth Sciences, 87, 247-257.

Schellart, W. P. (2008). Overriding plate shortening and extension above subduction zones: A parametric study to explain formation of the Andes Mountains. Geological Society of America Bulletin, 120(11-12), 1441-1454.

Schellart, W. P. (2020). Control of subduction zone age and size on flat slab subduction. Frontiers in Earth Science, 8, 26.

Scheuber, E., Reutter, K.J., 1992. Magmatic arc tectonics in the Central Andes between 21° and 25°S. Tectonophysics 205, 127-140. doi:10.1016/0040-1951(92)90422-3.

Schütte, P., Chiaradia, M., & Beate, B. (2010). Geodynamic controls on Tertiary arc magmatism in Ecuador: Constraints from U–Pb zircon geochronology of Oligocene–Miocene intrusions and regional age distribution trends. Tectonophysics, 489(1-4), 159-176.

SERNAGEOMIN, S. (2003). Mapa Geológico de Chile: versión digital. Servicio Nacional de Geología y Minería, Publicación Geológica Digital, No. 4 CD-Room, versión 1.0, base geológica escala, 1.

Skinner, S. M., Clayton, R. W. 2013. The lack of correlation between flat slabs and bathymetric impactors in South America. Earth and Planetary Science Letters 371:1-5.

Syracuse, E.M., Abers, G.A., 2006. Global compilation of variations in slab depth be-neath arc volcanoes and implications. Geochem. Geophys. Geosyst.7 (5), 73–90.

Syracuse EM, van Keken PE, Abers GA. 2010. The global range of subduction zone thermal models. Phys. Earth Planet. Inter. 183:73‑90

Scire, A., Biryol, C.B., Zandt, G., Beck, S., 2014. Imaging the Nazca slab and surrounding mantle to 700 km depth beneath the Central Andes (18°S to 28°S). Geological Society of America Memoirs 212, MWR212-02.

Scire, A., Zandt, G., Beck, S., Long, M., Wagner, L., Minaya, E., Tavera, H., 2015. Imaging the transition from flat to normal subduction: variations in the structure of the Nazca slab and upper mantle under southern Peru and northwestern Bolivia. Geophysical Journal International 204, 457-479. doi:10.1093/gji/ggv452.

Siks, B. C., & Horton, B. K. (2011). Growth and fragmentation of the Andean foreland basin during eastward advance of fold- thrust deformation, Puna plateau and Eastern Cordillera, northern Argentina. Tectonics, 30(6).

Silver, P. G., Russo, R. M., Lithgow-Bertelloni, C., 1998. Coupling of South American and African plate motion and plate deformation. Science 279(5347), 60-63.

Sobel, E.R., Hilley, G.E., Strecker, M.R. 2003. Formation of internally drained contractional basins by aridity-limited bedrock incision. Journal of Geophysical Resesearch, Solid Earth 108. http://dx.doi.org/10.1029/2002JB001883.

Somoza, R., 1998, Updated Nazca (Farallon)–South America relative motions during the last 40 My: Implications for mountain building in the central Andean region: Journal of South American Earth Sciences, v. 11, p. 211–215, doi:10.1016 /S0895-9811(98)00012-1.

Stern, C. R. (1991). Role of subduction erosion in the generation of Andean magmas. Geology, 19(1), 78-81.

Strecker, M.R., Hilley, G.E., Bookhagen, B., Sobel, E.R., 2012. Structural, Geomorphic, and Depositional Characteristics of Contiguous and Broken Foreland Basins: Examples from the Eastern Flanks of the Central Andes in Bolivia and NW Argentina. In: Tectonics of Sedimentary Basins, pp. 508–521.

Trumbull, R.B., Riller, U., Oncken, O., Scheuber, E., Munier, K., Hongn, F., 2006. The time-space distribution of Cenozoic volcanism in the South-Central Andes: a new data compilation and some tectonic implications, in: The Andes. Springer, pp. 29-43.

Vandervoort, D.S., Jordan, T.E., Zeitler, P., and Alonso, R.N., 1995, Chronology of internal drainage development and uplift, southern Puna Plateau, Argentine Central Andes: Geology, v. 23, p. 145–148, doi: 10.1130/0091-7613(1995)023<0145:COIDDA>2.3.CO;2.

Viramonte, J. G., and I. A. Petrinovic (1990), Cryptic and partially buried calderas along a strike-slip fault system in the Central Andes, ISAG Grenoble, edited by Inst. Français de Rech. Sci., pp. 317–320, Ed. de l’Orstom, Paris.

von Huene, R., Scholl, D.W., 1991. Observations at convergent margins concerning sediment subduction, subduction erosion, and the growth of continental crust. Rev. Geophys. 29, 279–316, doi: 10.1029/91RG00969.

Weil, A.B., Yonkee, W.A., and Kendall, J., 2014, Towards a better understanding of the influence of basement heterogeneities and lithospheric coupling on foreland deformation: A structural and paleomagnetic study of Laramide deformation in the southern Bighorn Arch: Geological Society of America Bulletin, v. 126, p. 415–437, https://doi.org/10.1130/B30872.1.

Wells, M. L., Hoisch, T. D., Cruz- Uribe, A. M., & Vervoort, J. D. (2012). Geodynamics of synconvergent extension and tectonic mode switching: Constraints from the Sevier-Laramide orogen. Tectonics, 31(1).

Winocur, D. A., Litvak, V. D., & Ramos, V. A. (2015). Magmatic and tectonic evolution of the Oligocene Valle del Cura basin, main Andes of Argentina and Chile: evidence for generalized extension. Geological Society, London, Special Publications, 399(1), 109-130.

Zapata, S., Sobel, E. R., del Papa, C., Jelinek, A. R., & Glodny, J. (2019a). Using a Paleosurface to Constrain Low-Temperature Thermochronological Data: Tectonic Evolution of the Cuevas Range, Central Andes. Tectonics, 38(11), 3939-3958.

Zapata, S., Sobel, E. R., del Papa, C., Muruaga, C., & Zhou, R. (2019b). Miocene fragmentation of the Central Andean foreland basins between 26 and 28° S. Journal of South American Earth Sciences, 94, 102238.

Zhou, R., Schoenbohm, L.M., Sobel, E.R., Stockli, D.F., and Glodny, J., 2014, Cooling history for the Sierra Laguna Blanca (NW Argentina) on the southern Puna Plateau, Central Andes: San Francisco, California, American Geophysical Union, Fall meeting supplement, abstract EP21A-3529.

Zhou, R., Schoenbohm, L.M., 2015. Late miocene upper-crustal deformation within the interior of the southern Puna plateau, Central Andes. Lithosphere 7, 336-352. doi:10.1130/l396.1. .

Zhou, R., Schoenbohm, L.M., Sobel, E.R., Carrapa, B., Davis, D.W., 2016a. Sedimentary record of regional deformation and dynamics of the thick-skinned southern Puna plateau, Central Andes (26º-27°S). Earth and Planetary Science Letters 433, 317-325. doi:10.1016/j.epsl.2015.11.012.

Zhou, R., Schoenbohm, L.M., Sobel, E.R., Davis, D.W., Glodny, J., 2016b. New constraints on orogenic models of the southern central andean plateau: Cenozoic basin evolution and bedrock exhumation. Geological Society of America Bulletin 129, 152-170. doi:10.1130/b31384.1.

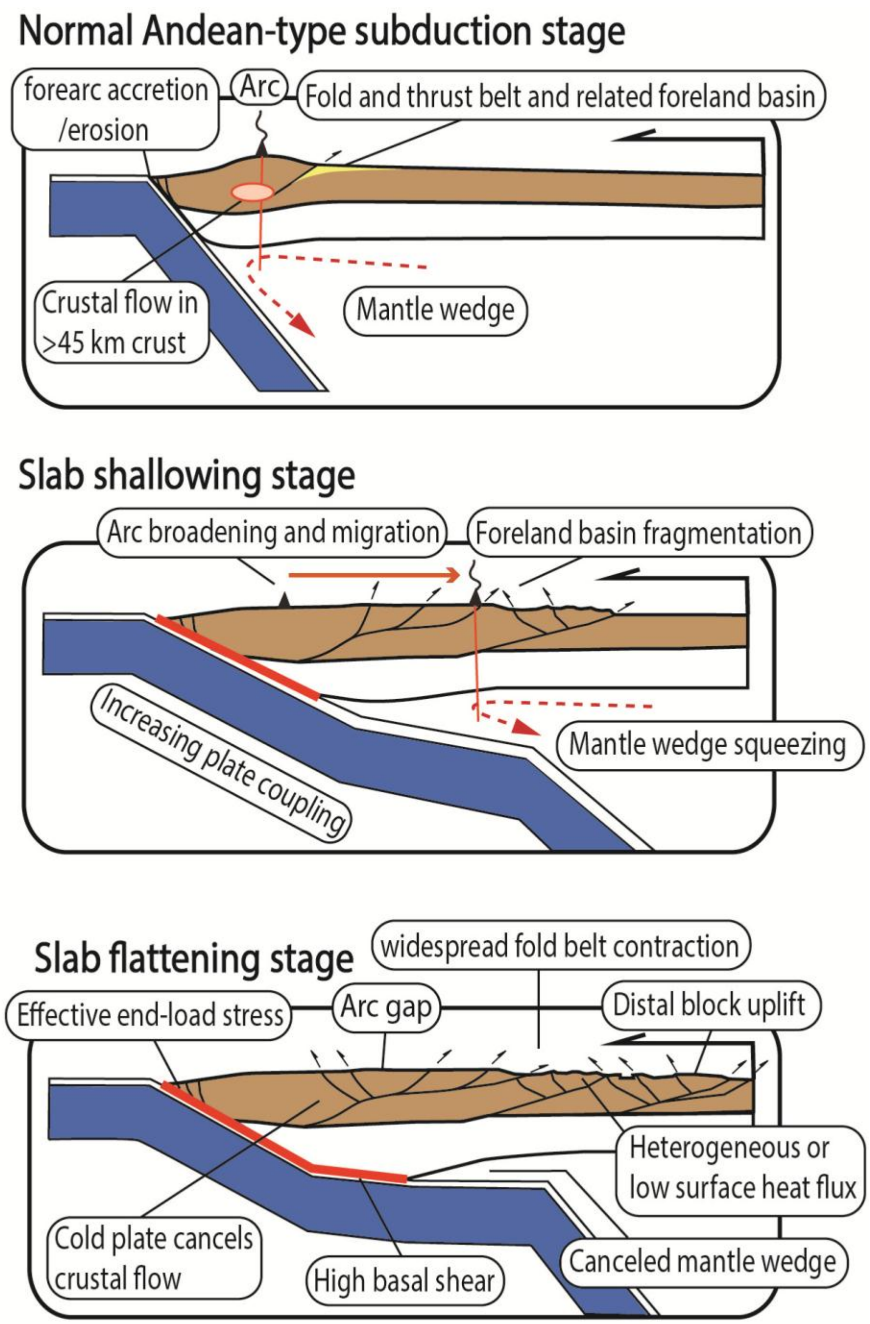

1046

1047 **Fig. 1**. Conceptual model of flat slab development and related tectonic, magmatic , and
1048 thermal modifications in the upper-plate based on Barazangui and Isacks (1976), Dickinson
1049 and Snyder (1978), Coney and Reynolds (1979) and Gutsher et al. (2000), Martinod et al.
1050 (2010), Ouimet and Cook (2010), and Axen et al. (2018).

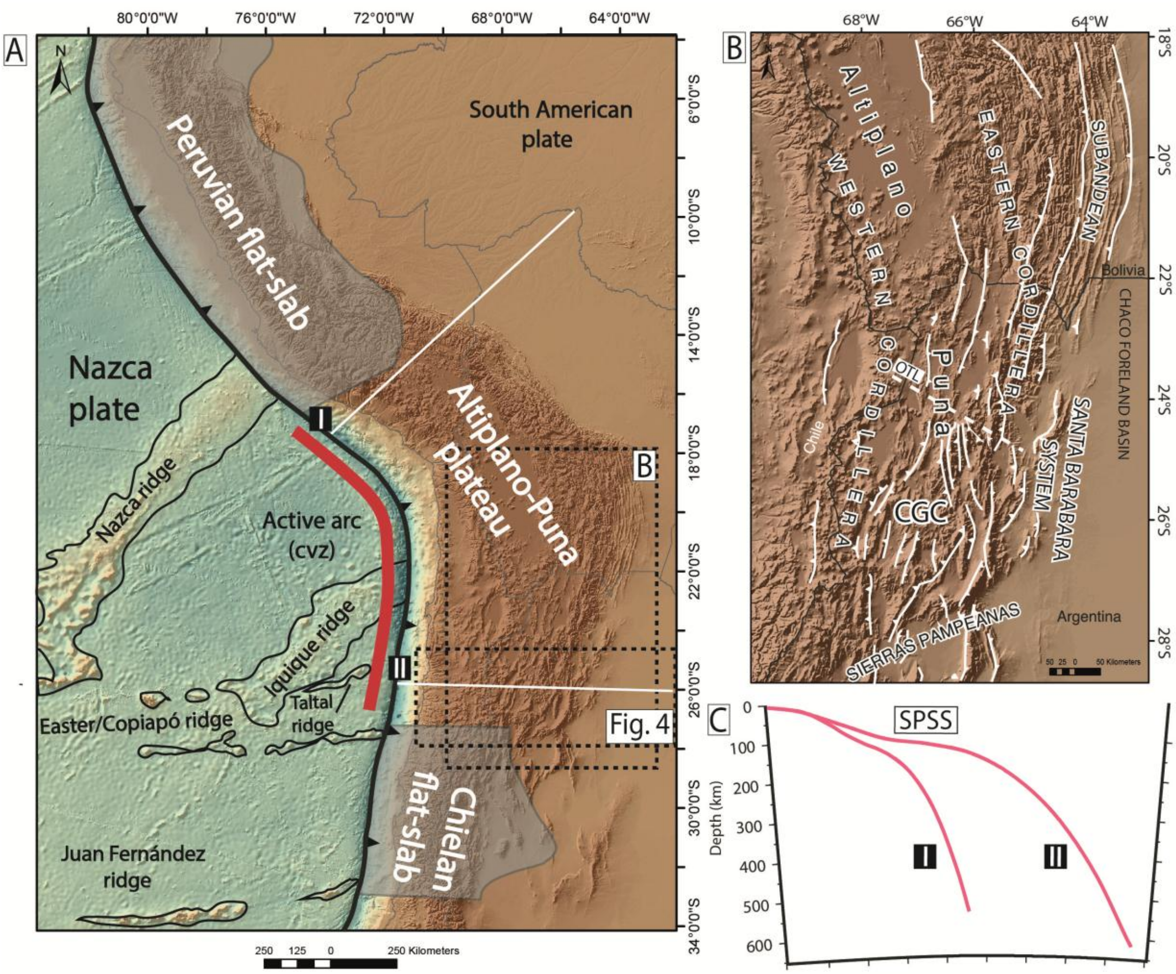

Fig. 2. (A) Tectonic setting of the Central Andes. Slab profiles are from the Slab2 model of Hayes et al. (2018). SPSS stands for southern Puna plateau subduction discussed in this study. (B) Image showing the Altiplano-Puna plateau and the southern Puna plateau south of the Olacapato-Toro lineament (OTL). CGC in stands for Cerro Galán caldera. (C) Subduction zone profiles from Hayes et al. (2018) in the northern and southern terminations of the CVZ.

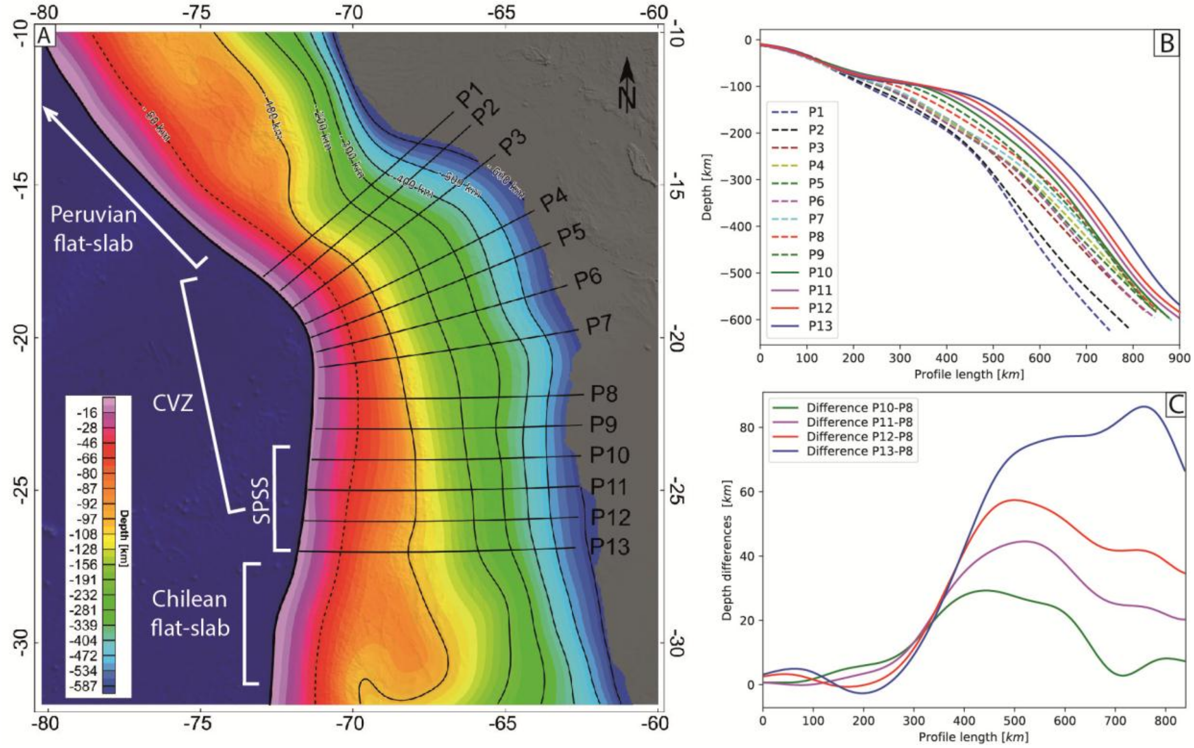

Fig. 3. (A) Depth map of the Nazca slab from the Slab2 model of Hayes et al. (2018). P1 to P13 indicate subduction profiles locations. SPSS stands for southern Puna shallow subduction discussed in this study. (B) Variation in subduction geometries along the CVZ showing progressive slab shallowing towards the southern Puna region. (C) Depth difference between profiles P10 to P13 and profile P8.

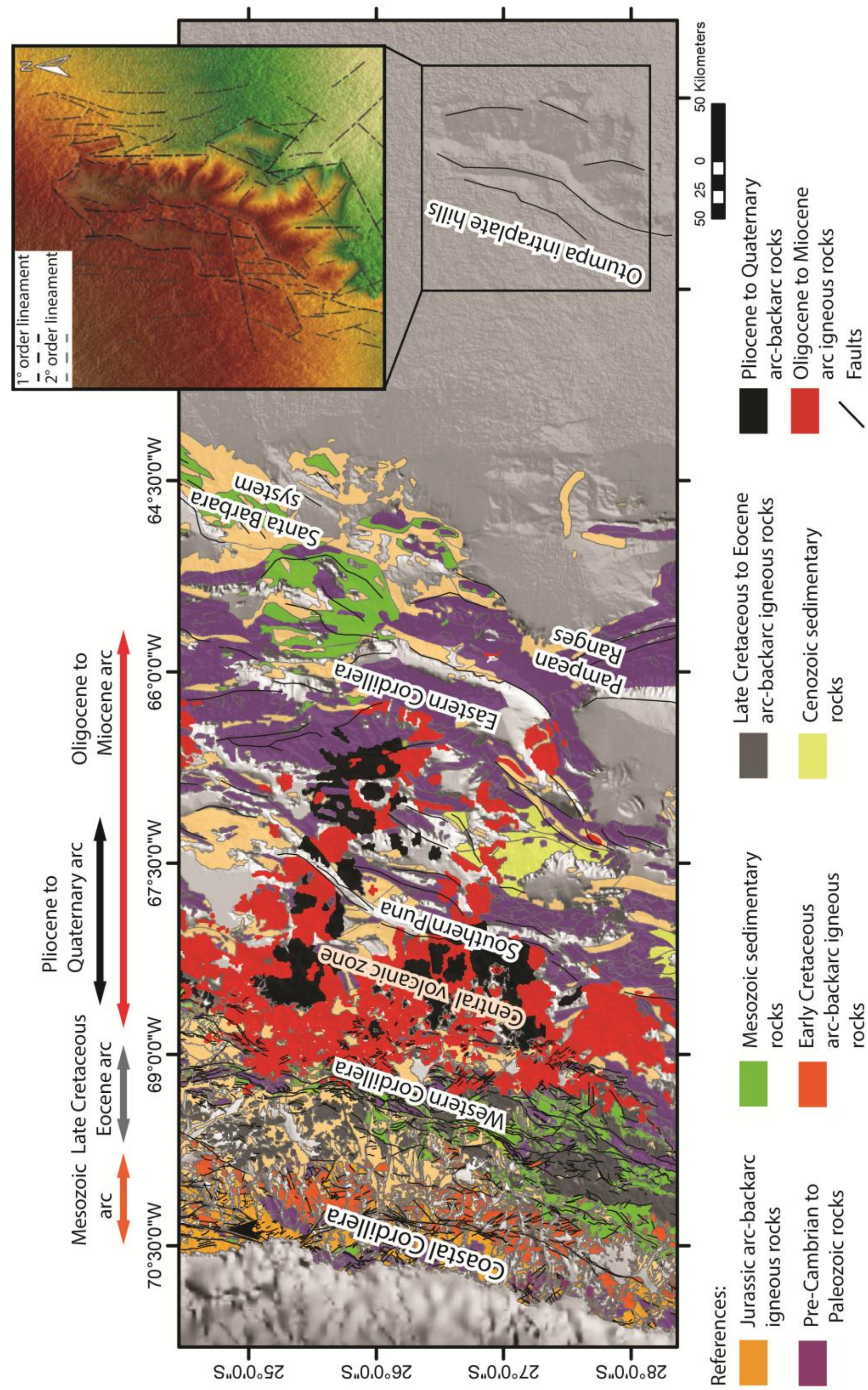

Fig. 4. Compiled regional geologic map based on SERNAGEOMIN (2003) and Caminos and González (1997) showing the main morphostructural units of the Central Andes. Note

the small stepwise migration of the Mesozoic arc, related to steady subduction erosion, and the significant arc expansion since Oligocene times here associated with the onset of the SPSS. Inset map of the Otumpa intraplate hills is modified from Peri (2012).

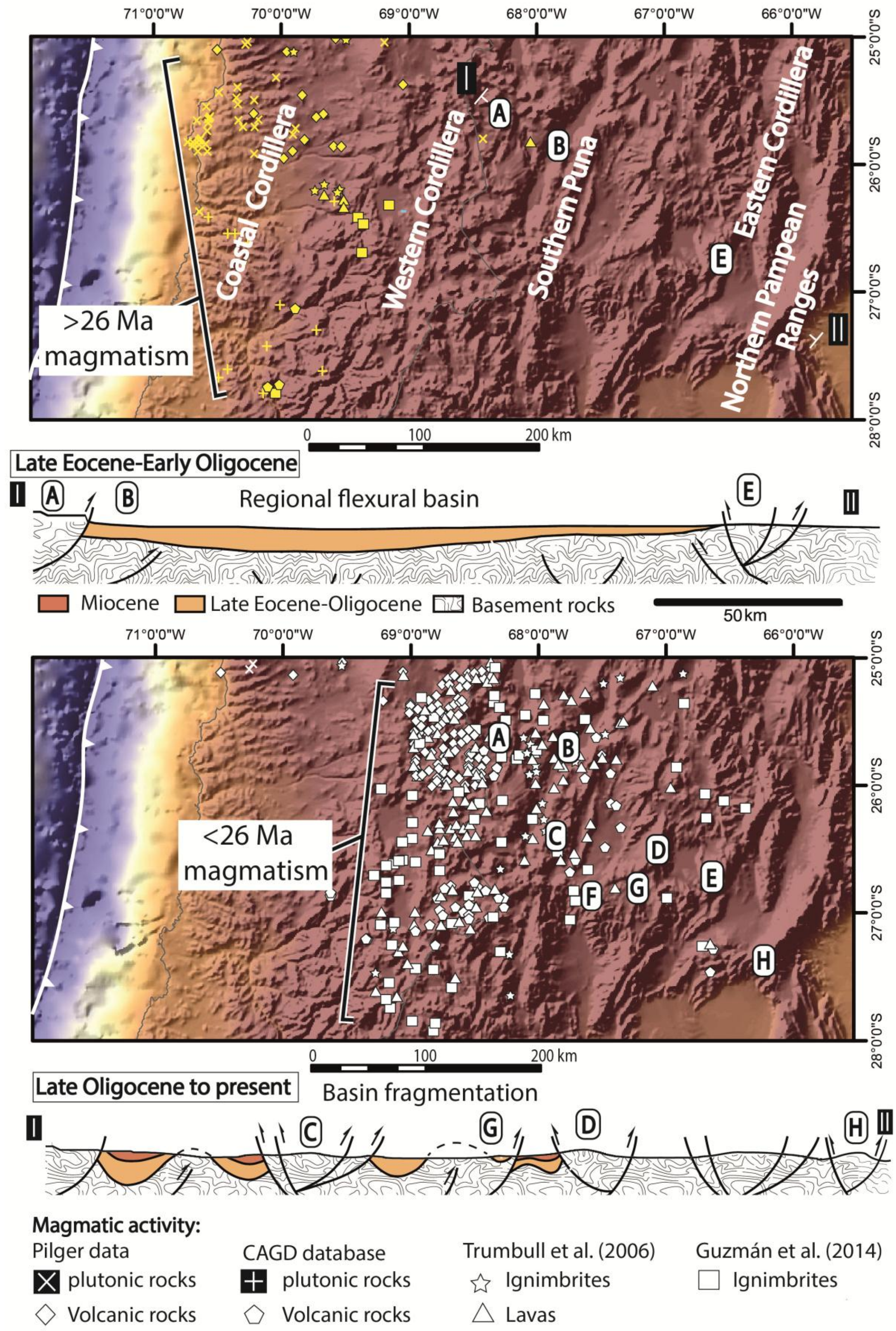

71°0'0"W
70°0'0"W
69°0'0"W
68°0'0"W
67°0'0"W
66°0'0"W
25°0'0"S
26°0'0"S
27°0'0"S
28°0'0"S
Coastal Cordillera
Western Cordillera
Southern Puna
Eastern Cordillera
Northern Pampean Ranges
>26 Ma magmatism
0
100
200 km
Late Eocene-Early Oligocene
Regional flexural basin
Miocene
Late Eocene-Oligocene
Basement rocks
50 km
<26 Ma magmatism
Late Oligocene to present
Basin fragmentation
Magmatic activity:
Pilger data
plutonic rocks
Volcanic rocks
CAGD database
plutonic rocks
Volcanic rocks
Trumbull et al. (2006)
Ignimbrites
Lavas
Guzmán et al. (2014)
Ignimbrites

Fig. 5. Data compilation of Andean magmatism from Guzmán et al. (2014), Trumbull et al. (2006), Pilger: http://www.pilger.us/id3.html, and CAGD: http://andes.gzg.geo.unigoettingen.de/ and tectonic evolution of the southern Puna Plateau displayed in generalized cross-sections at 26–27°S modified from Zhou et al. (2016a). Abbreviations are A: Sierra Quebrada Honda (Zhou et al., 2016b); B: Salar de Antofalla región (Kraemer et al., 1999; Canavan et al., 2014; Carrapa et al., 2005); C: Sierra de Calalaste (Carrapa et al., 2005; Zhou et al., 2016b); D: Sierra Laguna Blanca (Zhou et al., 2014); E: Sierra Chango Real (Coutand et al., 2001); F: Southern Puna margin (Carrapa et al., 2006); G: Pasto Ventura región (Zhou et al., 2016a); H: Northern Pampean Ranges.

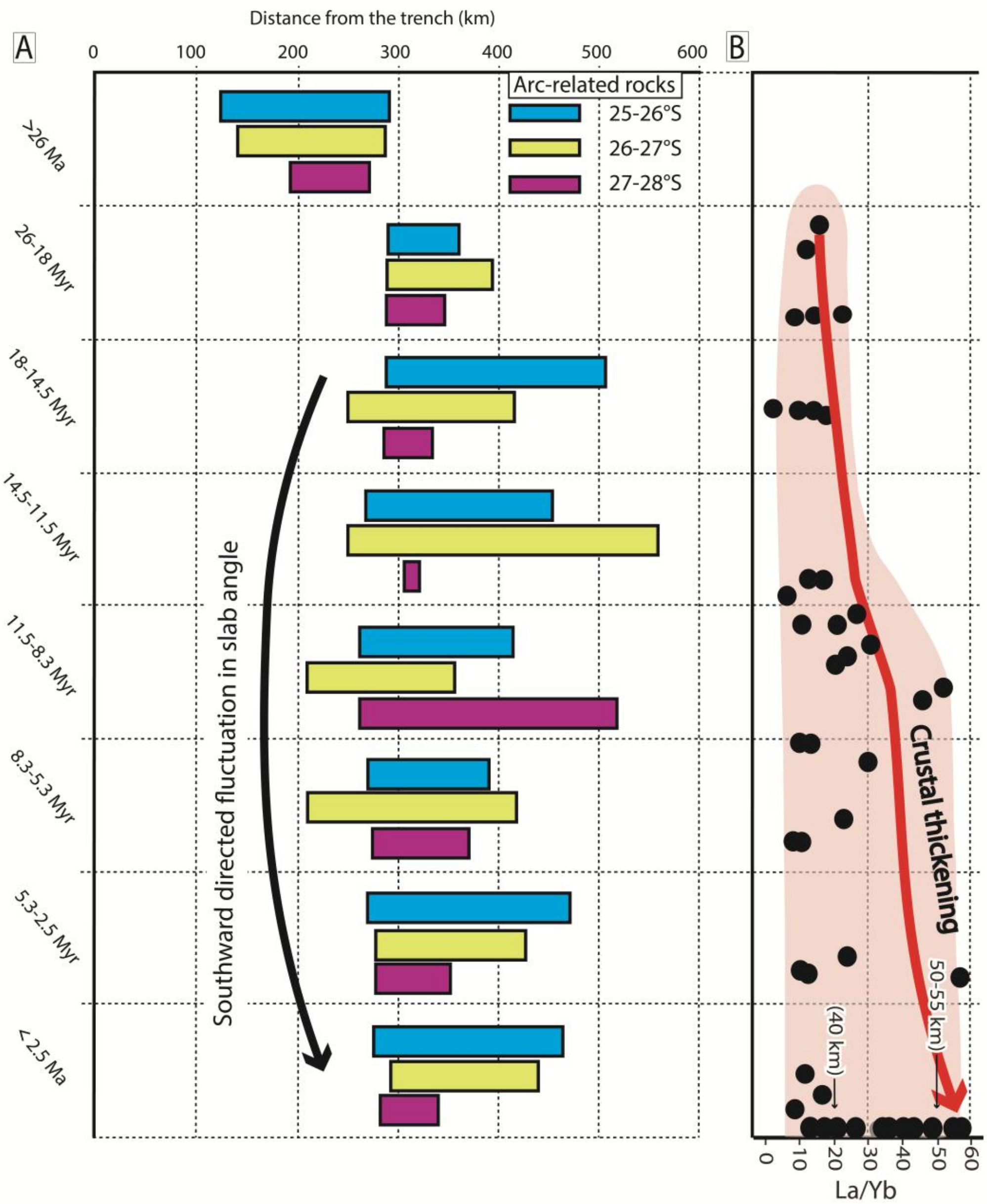

Fig. 6. (A) Spatio-temporal analysis of magmatism from Guzmán et al. (2014), after correction of 40 km of subduction erosion for rocks older than 8 Ma (Goss and Kay, 2009). (B) Crustal thickening after 26 Ma from Haschke et al. (2002) expressed by La/Yb ratios of Andean igneous rocks, which are thought to positively correlate with crustal thickness.

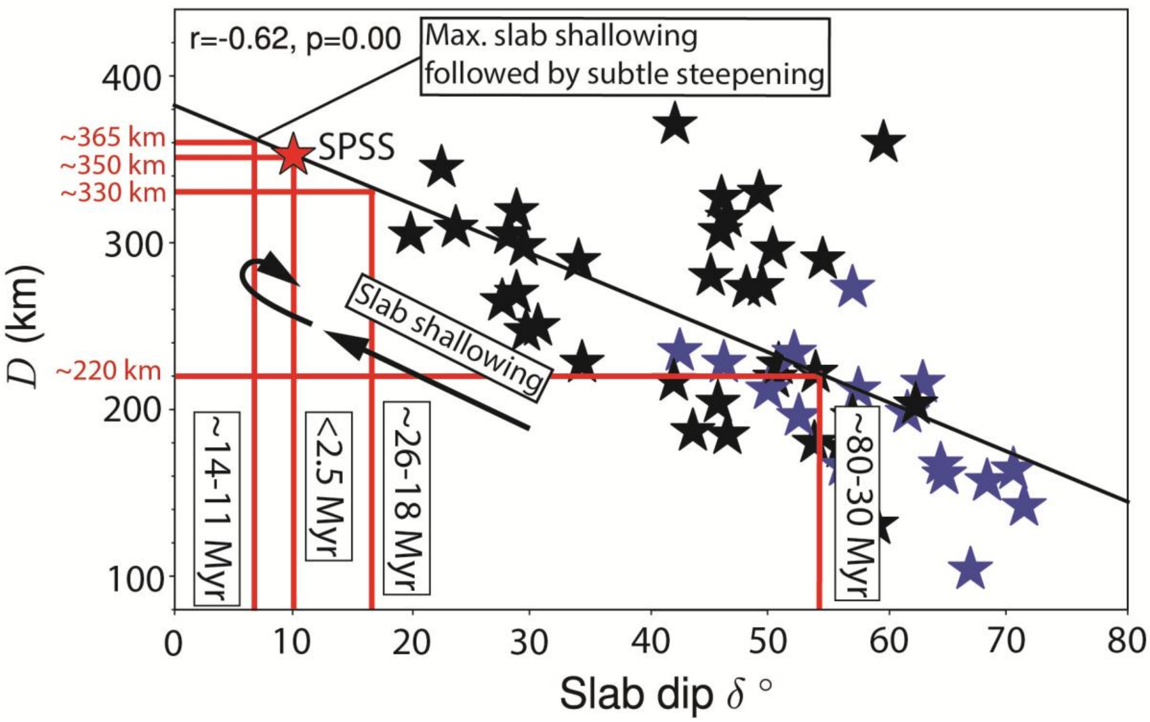

Fig. 7. Correlations between arc-trench distance D and slab dip modified from Perrin et al (2018) with plotted average D values for the three latitudinal segments in Fig. 6B (25-26°, 26-27°, and 27-28°) at 80-30 Myr, 26-18, 14-11 Myr and 2.5 Ma arc stages. Ocean–ocean subduction zones in blue symbols, ocean–continent zones in black. Black line is a linear fit to the complete dataset and **r** and **p** values represent correlation coefficients and the likelihood that no linear correlation exists, respectively. Stars are data from the global database of Syracuse et al. (2010). This diagram shows the potential evolution of slab dip through time depicting an over slab shallowing since 26 Ma. This process peaked at 14-11 Ma and is follwed by a subtle slab steepening achieving current shallow angles associated with the active SPSS.

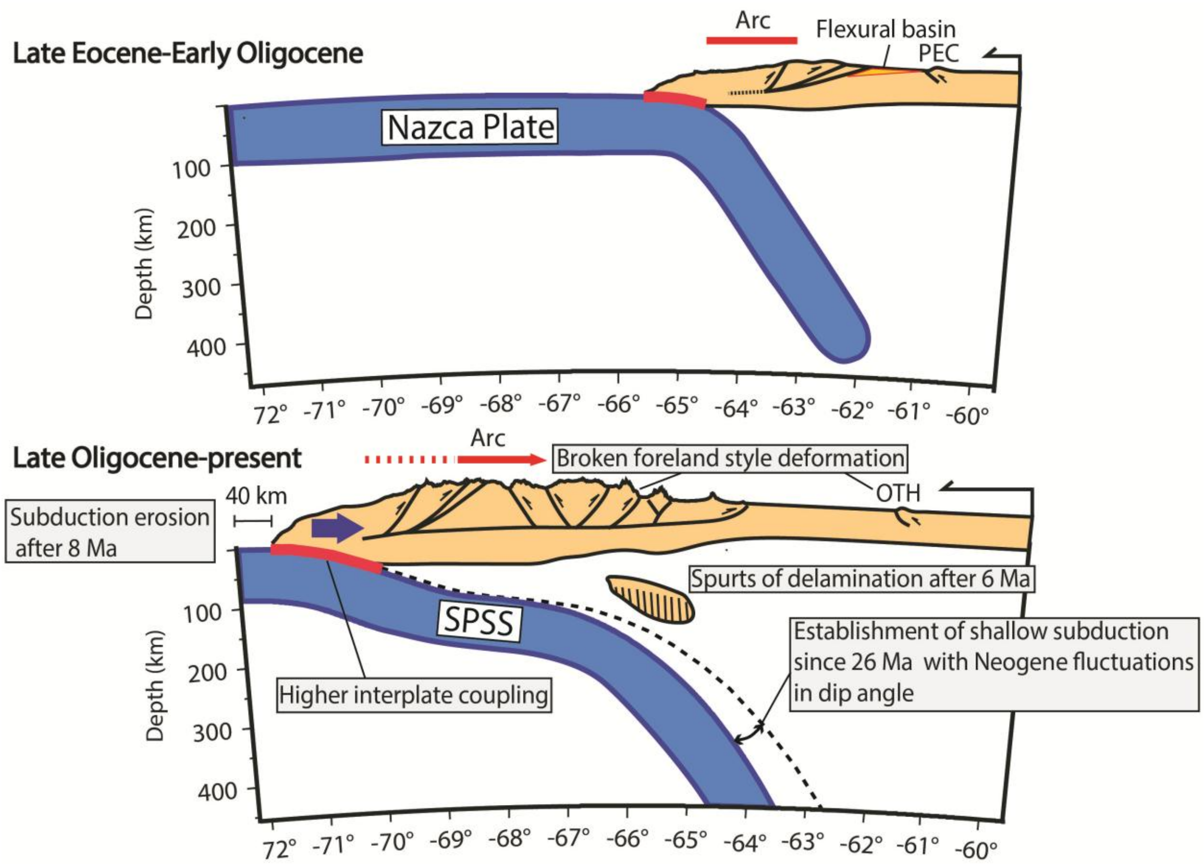

Fig. 8. Late Paleogene to present evolution of the southern Puna Plateau at 26ºS. See text for further details. Continental lithosphere not to scale. Abbreviations are PEC: Proto Eastern Cordillera, OTH: Otumpa intraplate Hills.